Atmos. Chem. Phys. Discuss., doi:10.5194/acp-2016-1011, 2017
Manuscript under review for journal Atmos. Chem. Phys.
Discussion started: 10 February 2017


Atmospheric Chemistry and Physics Discussions

# Impact of the choice of the satellite aerosol optical depth product in a sub-regional dust emission inversion

Jerónimo Escribano[1], Olivier Boucher[1], Frédéric Chevallier[2], and Nicolás Huneeus[3,4]

[1]Laboratoire de Météorologie Dynamique, Université Pierre et Marie Curie / CNRS, Paris, France
[2]Laboratoire des Sciences du Climat et de l'Environnement, CEA, Saclay, France
[3]Geophysics Department, University of Chile, Santiago, Chile
[4]Center for Climate and Resilience Research (CR)[2], Santiago, Chile

*Correspondence to:* Jerónimo Escribano (jeronimo.escribano@lmd.jussieu.fr)

**Abstract.**

Mineral dust is the major continental contributor to the global atmospheric aerosol burden with important effects on the climate system. Regionally, a large fraction of the emitted dust is produced in North Africa, however the total emission flux from this region is still highly uncertain. In order to reduce these uncertainties, emission estimates through top-down approaches (i.e., usually models constrained by observations) had been successfully developed and implemented. Such studies usually rely on a single observational dataset and propagate the possible observational errors of this dataset onto the emission estimates. In this study, aerosol optical depth (AOD) products from five different satellites are assimilated one by one in a source inversion system to estimate dust emission fluxes over northern Africa and the Arabian Peninsula. We estimate mineral dust emissions for the year 2006 and discuss the impact of the assimilated dataset on the analysis. We find a relatively large dispersion in flux estimates among the five experiments, which can likely be attributed to differences in the assimilated observation datasets and their associated error statistics. We also show how the assimilation of a variety of AOD products can help to identify systematic errors in models.

## 1 Introduction

Aerosol optical depth (AOD) retrieved from satellites is probably the most used indirect measurement of aerosol in atmospheric and climate modelling studies. The large temporal and spatial coverage of satellite AOD makes these retrievals a unique and useful product, however they cannot provide a complete four-dimensional description of the atmospheric aerosol. Data assimilation techniques have been developed to combine in the best possible way model and observational information and their application results in new aerosol analysis and reanalysis products (e.g., Benedetti et al., 2009; Lynch et al., 2016). In the recent years, satellite-derived AOD has been also used to estimate aerosol surface emissions in the so-called *top-down* approach (e.g., Dubovik et al., 2008; Schutgens et al., 2012; Huneeus et al., 2012). This approach is often embedded in a data assimilation framework, where observations and model are systematically combined in order to estimate emissions. With these methodologies, estimates of aerosol emissions depends on the model performance, on the detail of the data assimilation system and on the quality and coverage of the observations.

Atmos. Chem. Phys. Discuss., doi:10.5194/acp-2016-1011, 2017
Manuscript under review for journal Atmos. Chem. Phys.
Discussion started: 10 February 2017


Atmospheric Chemistry and Physics Discussions

Mineral dust is the major continental contributor to the global atmospheric aerosol burden. Airborne dust interacts with clouds, solar and terrestrial radiation and atmospheric chemistry. Deposition over the cryosphere has effects on surface albedo (Bond et al., 2013), which modulates the impact of black carbon deposition on snow and ice surfaces. Dust is a source of Fe and P nutrients. The deposition of dust on some continental ecosystems has some impact on the vegetation and the carbon cycle. Deposition at the surface of the oceans can also fertilize the phytoplankton in so-called high-nutrient low-chlorophyll regions, with impacts on marine biogeochemical cycles (Wang et al., 2015). Atmospheric dust is also known to affect human health and air quality. Among others uncertainties, emission fluxes of mineral dust are still highly uncertain. For instance dust emissions from the Saharan desert, a key dust region worldwide, have been estimated to range between 400 $\mathrm{Tg\,yr^{-1}}$ (e.g., Huneeus et al., 2011) to 4500 $\mathrm{Tg\,yr^{-1}}$ (e.g., Evan et al., 2014). While some of the uncertainty may be related to the choice of the cut-off size for dust emissions, with larger cut-off size resulting in larger dust emission fluxes and shorter atmospheric residence time, it is nevertheless desirable to decrease the uncertainty in the dust emission flux.

Satellite observations can help reducing these emission uncertainties. The combined use of satellite observations and models may potentially lead to superior estimates of aerosol emissions (e.g. Dubovik et al., 2008; Huneeus et al., 2012). In this study we focus on the role of observations and we quantify the plausible range of emissions uncertainties as a function of the chosen observational dataset. To this aim, we assimilate AOD from five different datasets in the data assimilation system presented in Escribano et al. (2016, hereafter EBCH16) with a fixed configuration for both the model and the assimilation system.

Moderate Resolution Imaging Spectroradiometer (MODIS) aerosol products have been largely used for aerosol data assimilation (e.g., Dubovik et al., 2008; Benedetti et al., 2009; Lynch et al., 2016, EBCH16). This is not surprising because the MODIS aerosol retrieval algorithms have received a lot of attention for over a decade (e.g., Remer et al., 2005, 2008; Levy et al., 2010) and, as a result, the MODIS aerosol products are of a relatively high quality (Levy et al., 2013). Over ocean and dark land surfaces, the MODIS Dark Target (MODIS-DT) algorithm is capable of retrieving AOD at visible wavelengths, while over bright surfaces AOD is retrieved through the MODIS Deep Blue (MODIS-DB) algorithm. Furthermore the MODIS instrument is onboard both the Aqua and Terra satellites, with morning and afternoon overpasses respectively, allowing for a large temporal and spatial coverage. However MODIS products are not totally free of problems. Sayer et al. (2013) evaluated the latest collection of MODIS Deep Blue aerosol product and found a low bias in AOD over the Sahara Desert. On the contrary, it is possible that MODIS-DT is biased high over the ocean, at least in dust outflow regions (Levy et al., 2003).

Aerosol products from other satellite sensors are also suitable for use in aerosol data assimilation. In the visible spectrum, this includes aerosol products from several instruments onboard low-Earth orbiting satellites like the Multiangle Imaging Spectroradiometer (MISR), Polarization and Anisotropy of Reflectances for Atmospheric Sciences Coupled with Observations from a Lidar (PARASOL), Advanced Along-Track Scanning Radiometer (AATSR) and Visible/Infrared Imaging Radiometer Suite (VIIRS). From geoestationary satellites, AOD is available from the Spinning Enhanced Visible and Infrared Imager (SEVIRI) instrument onboard Meteosat Second Generation (MSG) and the Advanced Himawari Imager (AHI) onboard the Japanese geostationary meteorological satellite Himawari-8. In the infrared, aerosol products are available from the Advanced Infrared Radiation Sounder (AIRS) and the Infrared Atmospheric Sounder Interferometer (IASI) instruments, particularly for dust aerosols that have a strong signature in the longer wavelengths. Finally it is also possible to assimilate the vertical profile

Atmos. Chem. Phys. Discuss., doi:10.5194/acp-2016-1011, 2017
Manuscript under review for journal Atmos. Chem. Phys.
Discussion started: 10 February 2017


Atmospheric Chemistry and Physics Discussions

of the extinction coefficient from the Cloud-Aerosol Lidar with Orthogonal Polarization (CALIOP) sensor onboard the Cloud-Aerosol Lidar and Infrared Pathfinder Satellite Observation (CALIPSO) mission but this is also fraught with difficulties as such inversion is fairly sensitive to assumptions made on the aerosol model.

An evaluation of some of these products is done in de Leeuw et al. (2015). The authors found that most of the compared satellite products have a good performance of AOD retrievals with respect to ground-based AOD measurements. In theory it should be possible to take advantage of their complementarity either in terms of aerosol information content or in terms of temporal and spatial coverage. In practice, assimilating several aerosol products simultaneously is fraught with difficulties because the satellite products may be inconsistent with each other, or inconsistent with the aerosol model. To our knowledge there are few (e.g., Saide et al., 2014; Zhang et al., 2014) data assimilation studies that seek to combine different aerosol products.

In EBCH16 we described an inversion system and presented a dust source inversion for North Africa assimilating 550 $\mathrm{nm}$ AOD from the MODIS/Aqua instrument. We now broaden the analysis and consider several retrieval products. Rather than combining different aerosol products, we seek to understand how different aerosol products perform on their own in the data assimilation system, in order to assess the strengths and weaknesses of each aerosol dataset in the context of Saharan dust and possible inconsistencies between the products. We thus compare the assimilation of five satellite AOD retrievals with the aim to narrow uncertainties in dust emission estimates for North Africa and the Arabian Peninsula.

The next Section presents the assimilated observations and the observations used in the validation. The assimilation system is briefly described in Sect. 2, the main results and mineral dust flux estimates are shown in Sect. 3. We finish this work with our conclusions in Sect. 4.

## 2 Inversion system

### 2.1 Observation operator

The observation operator is described in EBCH16 and references therein. As a brief summary, the observation operator consists of the AOD estimation given by the coupling of the LMDz meteorological model (Hourdin et al., 2013) with a simplified aerosol model (Huneeus et al., 2009, hereafter referres as SPLA). The dust emissions are calculated as in EBCH16, which itself follows the Alfaro and Gomes (2001) and Marticorena and Bergametti (1995) emission scheme. The SPLA model is an Eulerian aerosol model of intermediate complexity (Huneeus et al., 2009) with four aerosol species (fine mode aerosols, coarse sea salt, coarse mineral dust and super-coarse mineral dust) and one tracer for gaseous aerosol precursors. In this model we parameterized the processes of boundary layer mixing, dry and wet deposition and sedimentation (for coarser particles). In the model, mineral dust aerosol are emitted in three bins. Fine mode dust has diameter less than 1 $\mu\mathrm{m}$, coarse dust has diameter between 1 $\mu\mathrm{m}$ and 6 $\mu\mathrm{m}$ and super-coarse dust is between 6 $\mu\mathrm{m}$ and 30 $\mu\mathrm{m}$ in diameter. Once in the atmosphere, coarse and super-coarse dust are both independent model species, while fine dust is treated in the fine mode aerosols tracer. A detailed description of the aerosol model is provided in Huneeus et al. (2009) and updated in EBCH16.

Atmos. Chem. Phys. Discuss., doi:10.5194/acp-2016-1011, 2017
Manuscript under review for journal Atmos. Chem. Phys.
Discussion started: 10 February 2017


Atmospheric Chemistry and Physics Discussions

In this work, the model has been configured with 39 vertical levels, and with an horizontal zoom centered over North Africa. The horizontal resolution over North Africa is approximately 1° by 1°, and the average horizontal resolution in between 70°W and 70°E; and 0°N and 40°N is approximately 1° in latitude and 1.4° in longitude. The one-year spin-up and the model simulations for the year 2006 where performed with a wind nudging from ERA-Intermim reanalysis (Dee et al., 2011) as is explained in EBCH16.

### 2.2 Control vector

The control vector is composed of multiplicative correction factors of the model emissions as in EBCH16. These correction factors are assumed homogeneous for each element of a partition of the emission flux in space (sub-regions), time (sub-periods) and type of aerosol (categories). Five categories of emissions are defined (as in EBCH16) namely i) sea salt, ii) biomass burning emissions, iii) fine dust and coarse dust, iv) super-coarse dust, and v) fossil fuel and anthropogenic $SO_2$ emissions. In this work, correction factors of fine dust and coarse dust are lumped together, while super-coarse dust has separate correction factors. Preliminary test have shown low sensitivity of the analysis to the to the grouping of the three dust correction factors in only two, either fine and coarse dust together and supercoarse independent (as in this work) or coarse and super-coarse dust lumped together and fine dust independent (as in EBCH16). Additionally, our test show that if the three dust correction factors are independent elements in the control vector, the assimilation results do not improve and the computational burden increases.

Sub-regions are defined depending on the emission category and they are the same as in EBCH16. For fossil fuel and anthropogenic $SO_2$ emissions and for sea salt emissions only one global sub-region is considered. For biomass burning emissions, two sub-regions have been defined, according to a grass-like and forest-like land cover maps. For both categories of mineral dust, 19 sub-regions are been defined: 15 of the over northern Africa, 3 of them over the Arabian Peninsula and Middle East and one sub-region for the rest of the globe. We refer to Fig. 1 of EBCH16 for a map of the dust sub-regions.

The correction factors are assumed constant within each sub-period. Like EBCH16, sea salt has a sub-period of one year, biomass burning and fossil fuel and anthropogenic $SO_2$ emissions have a sub-period of one month. A substantial difference with EBCH16 is the length of the sub-period for dust emissions. It was set to one month in EBCH16 but is reduced in this work to only three days. With this shorter sub-period (corresponding to the sub-synoptic to synoptic scale), we expect to better capture the dust emission variability in the analysis. This results in a control vector of 4674 components (that is about 10 times larger than in EBCH16), which required some modifications in how to deal with the inversion matrices. The later is mainly relates to technical concerns, as carefully avoid numerical errors in matrices multiplication and inversions, the use of efficient algorithms to ensure semi positiveness of some matrices involved in the inversion, and a satisfactory computational memory management of these large matrices.

### 2.3 Observations

In addition to the MODIS/Aqua total 550-nm AOD retrievals that we used in EBCH16, we now also assimilate fine mode 550-nm AOD over ocean in this study. Furthermore we consider a range of other aerosol products from passive instruments measuring solar reflectances. We do not consider aerosol products from passive instruments operating in the infrared or from



active instruments as they would require different observational operators, which would introduce further complications in the interpretation of the results.

MODIS/Terra is a MODIS instrument on-board the low Earth orbiting satellite Terra (with equatorial overpass around 10:30 Local Time). The AOD retrievals from MODIS/Terra are calculated with the same algorithms than for MODIS/Aqua (Levy et al. (2013); Sayer et al. (2013, 2014)) providing total 550-nm AOD over land (Deep Blue and Dark Target algorithms) and fine mode and total 550-nm AOD over ocean (Dark Target algorithm only). We use the Level 3 AOD merged product from the Collection 6 for MODIS/Terra and MODIS/Aqua.

The POLarization and Directionality of the Earth's Reflectances instrument (POLDER, Tanré et al., 2011) onboard the PARASOL satellite measures radiances in 9 narrow channels in the visible to near-infrared spectrum with up to 16 viewing geometries and information on polarization in 3 of the channels. Through an advanced algorithm it reports total 670 and 865-nm AOD over ocean and the 865 nm fine AOD over land with their corresponding Ångström coefficient. Using this coefficient we derive the 550-nm AOD from these retrievals, for total and fine mode over ocean and fine mode over land. During year 2006, this instrument was orbiting in the "A-Train" along with the Aqua satellite. As the swath of the POLDER instrument onboard PARASOL (1600 km) is relatively close to that of MODIS (2330 km), PARASOL and MODIS/Aqua have fairly similar spatial and temporal coverage although the two algorithms differ in the clear-sky mask they use, and hence on the spatial coverage of the AOD products.

The MISR instrument onboard the Terra satellite reports 555 nm AOD over land and ocean (Kahn et al., 2009). The MISR algorithm uses multi-angular and multi-spectral information to retrieve the AOD. The swath of this instrument is smaller than the swath of MODIS which results in less coverage. Specifically, the standard Level 2 (individual soundings) and Level 3 (daily mean maps) MISR products report 555 nm AOD for fine (less than 0.7 µm of diameter), medium (between 0.7 and 1.4 µm of diameter) and large (more than 1.4 µm of diameter) aerosols. Regrettably, the size cut-off between the MISR products and the SPLA model are not compatible so we need to post-process the MISR products before assimilation. We do it in the following way. The MISR retrieval algorithm calculates the best linear combination of 74 aerosol *mixture* models in order to fit the measured radiances for each observed pixel. These fitting parameters and the main parameters of the aerosol models are reported in Level 2 of the MISR products. With this information and with the reported Level 2 AOD, we have calculated an estimate of the MISR 555 nm AODs with the same diameter cut-off than the SPLA model, i.e., for fine (less than 1 µm of diameter), coarse (between 1 and 6 µm of diameter) and super-coarse (larger than 6 µm of diameter) aerosols. Briefly, the post-processing of the MISR AOD was the following: (i) we calculated the contribution of each aerosol model to the total AOD, using the reported fitting parameters and considering the 8 *basic* aerosol models of MISR algorithm; (ii) assuming that the reported extinction coefficient for each model is independent from the size distribution, we estimated the contribution of each bin (as the SPLA definitions) to the total AOD. In practice, our approximation of the AOD reprojected on the three modes of the SPLA model is accurate with a relative error of (maximum) 5% of the total AOD for the 5% less accurate recomputed retrievals. In this work we only used the recomputed fine mode and total 555-nm MISR AOD.

The AERUS-GEO product (Aerosol and surface albEdo Retrieval Using a directional Splitting method-application to GEO-stationary data, Carrer et al., 2010, 2014) is a full-disk daily 630 nm AOD retrieval calculated from the measured radiances

Atmos. Chem. Phys. Discuss., doi:10.5194/acp-2016-1011, 2017
Manuscript under review for journal Atmos. Chem. Phys.
Discussion started: 10 February 2017


Atmospheric Chemistry and Physics Discussions

of the SEVIRI instrument. These retrievals cover Europe and Africa. Unlike the above mentioned products, AERUS-GEO uses only one spectral band to calculate the daily AOD product, based on measurements done in a relatively high spatial and temporal resolution in different (i.e. time-varying) conditions of solar angles. The native spatial resolution of this product is 3 km by 3 km close to the Equator. We use the total 630 nm AOD from this product. We have screened all the pixels where the "ZAge" flag of the product is greater than zero [D. Carrer, personal communication]. This filter removes suspicious large and persistent AOD values in the equatorial Atlantic ocean which are related to a time persistency assumption in the algorithm. After this screening, the 80 % of the full-disk valid data is kept over land and the 56 % over ocean.

Most common regridding techniques have problems handling missing data (e.g. bilinear interpolation) or can be inaccurate when the spatial resolutions of the input and output grids are too different (e.g. nearest neighbour). In the present work the regridding of all AOD satellite products into the model grid was performed with a weighted-area procedure. Furthermore only the model grid-boxes covered with 30% or more of satellite valid data are considered; they are otherwise set to a missing value. This arbitrary value of 30% approximately propagates the same coverage area of the satellite products into the model grid. This regridding method successfully handles the missing values and large differences in grid resolutions. Moreover, if the input field has no missing values and both are latitude-longitude grids, this method is equivalent to a bilinear interpolation.

Figure 1 shows the average AOD for the year 2006 for each instrument described above. It is important to note the difference in the sampling time of each product. The SEVIRI product is retrieved using a combination of all the available observations per day, thus achieving a mean coverage of 75% per day in our assimilation region for the year 2006. The low Earth orbiting satellites typically sample only once per day our region of interest coverage. However MISR has a more narrow swath than MODIS and POLDER (on PARASOL) so its coverage is less. We say more about the number of observations in the next Section.

### 2.4 Error covariance matrices and assimilation configuration

The covariance matrix of the background errors **B** is defined with similar values to the ones from EBCH16. The standard deviation of the control vector errors (i.e. the square root of the diagonal terms of **B**) are 1.3 for for biomass burning emissions, 3.0 for mineral dust emissions, 2.0 for sea salt emissions and 0.18 for anthropogenic and fossil fuel emissions. We have included correlations between control vector errors. For the same sub-region and category of dust emission (fine and coarse dust, super-coarse dust) we have defined a Gaussian correlation between sub-periods with a time-length scale of three days. In comparison with EBCH16, this shortened timescale giving more freedom to the assimilation system. It allows the assimilation system to take advantage of the shortened sub-period, with the aim of improving the representation of dust events at these scales. Furthermore, the shorter sub-period of the dust control vector of this work compared to EBCH16 (3 days versus 1 month) raises the size of the control vector from 494 to 4,674 elements. For the same sub-region and sub-period, the correlation of errors between the fine and coarse dust emission correction factors and the super-coarse correction factor is set to 0.7.

A substantial difference with EBCH16 is the construction of the covariance matrix of the observational errors (**R**). In EBCH16 the standard deviation of the observational errors were set to a fixed value of 0.2 and 0.1 for MODIS AOD products over land and ocean, respectively. In this work we keep a diagonal **R** matrix but the errors are defined according to the obser-

Atmos. Chem. Phys. Discuss., doi:10.5194/acp-2016-1011, 2017
Manuscript under review for journal Atmos. Chem. Phys.
Discussion started: 10 February 2017


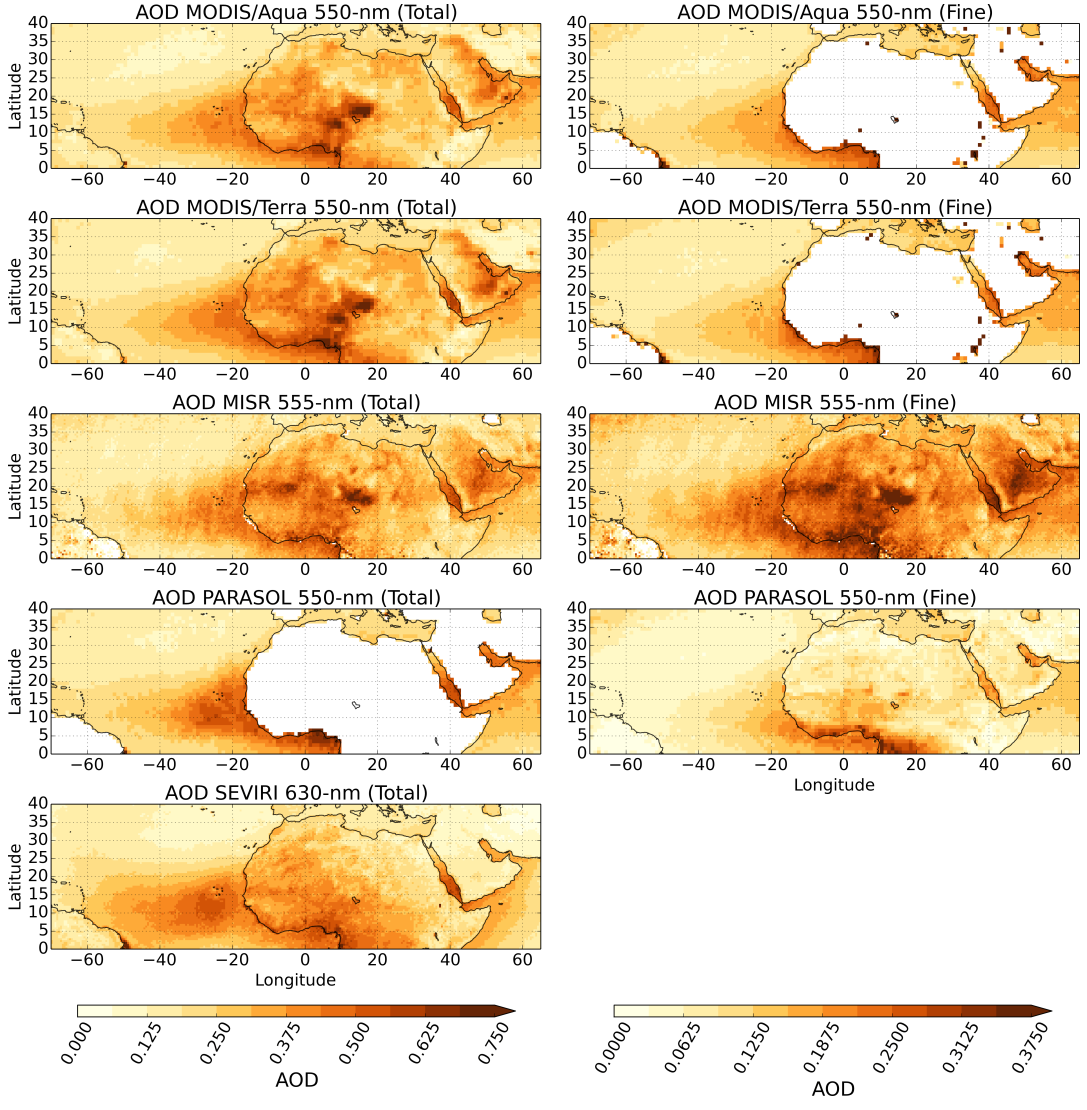


**Figure 1.** Averages for the year 2006 of the satellite-derived AOD products used in this study. The AOD products are all regridded to a regular latitude-longitude grid of 0.5° resolution for MISR and SEVIRI and 1° for MODIS and PARASOL. The total AOD is shown on the left column and the fine mode AOD (when available) on the right column. Please note that the different color scales between the two columns and the (somewhat) different wavelengths of the reported AOD.

vational errors reported in the literature. A summary of these definitions is shown in Table 1. For the sake of simplicity, the errors were calculated using the satellite AOD as the reference AOD, despite the fact that most of the derivations of these error formulae were done using an independent AOD dataset as a reference. The standard deviation of the observational errors have to be prescribed to the data assimilation system. For MODIS and MISR, the errors are characterized by an *expected error* (EE) which defines the boundaries of a region that contains the 67% of the matchups between the satellite AOD and the reference

Atmos. Chem. Phys. Discuss., doi:10.5194/acp-2016-1011, 2017
Manuscript under review for journal Atmos. Chem. Phys.
Discussion started: 10 February 2017


Atmospheric Chemistry and Physics Discussions

**Table 1.** Definitions of diagonal terms in the observational error covariance matrix. The main references for the errors are shown in the table. The original error formulae were adapted for the assimilation purposes. The error shown for MODIS-DT over land is not used in this work. Errors for the SEVIRI dataset ($C_k$) are described in Carrer et al. (2010, 2014).

| Dataset | Error estimate (from reference) | Error adapted to this work | Reference |
|---|---|---|---|
| MODIS-DB | $\pm(0.03+0.2\tau)$ | $0.03+0.2\tau$ | Sayer et al. (2013) |
| MODIS-DT ocean | $[-(0.02+0.1\tau),+(0.04+0.1\tau)]$ | $0.03+0.1\tau$ | Levy et al. (2013) |
| MODIS-DT land | $\pm(0.05+0.15\tau)$ | $0.05+0.15\tau$ | Levy et al. (2013) |
| MISR | $\pm\max(0.05,0.2\tau)$ | $\max(0.05,0.2\tau)$ | Kahn et al. (2005) |
| PARASOL | $\pm0.05\pm0.05\tau$ | $\sqrt{0.05^2+(0.05\tau)^2}$ | Tanré et al. (2011) |
| SEVIRI | $\sqrt{C_k}$ | $\sqrt{C_k}$ | Carrer et al. (2010, 2014) |

AOD. For the MODIS merged product over land there is no equivalent error quantification. In this work, the majority of the assimilated observations over land are over North Africa and the Arabian Peninsula, where most of the AOD is retrieved by the MODIS-DB algorithm. Hence, we adopt MODIS-DB error quantification as the standard deviation for MODIS land AOD. Over ocean, the MODIS merged AOD is the same as the Dark Target product, but the DT EE is not centered on zero. We adopt the approximation shown in Table 1 for MODIS over ocean, shifting the EE to be symmetrical around zero at their minima. For PARASOL AOD, we assume that both terms shown in Table 1 are independent and Gaussian distributed in order to calculate the error estimate for the data assimilation system. Due to the lack of separate error estimates of fine AOD, we assume the error estimates of Table 1 for fine AOD of MODIS, MISR and PARASOL. SEVIRI reports pixel-wise variance of the errors which are themselves the diagonal elements of the covariance matrix of the analysis errors in the AERUS-GEO retrieval algorithm. As we do not have information about the correlation of the errors of nearby pixels, we compute the regridded SEVIRI AOD error assuming that all the SEVIRI pixels in the native grid are fully correlated within each model gridbox. In our case this assumption conserves the spatial structure of the AOD errors. This is done only for SEVIRI AOD, as they report pixel-wise AOD error variance in their daily product.

Unlike EBCH16, we do not inflate the covariance matrices in order to fulfill the Desroziers et al. (2005) diagnostics. Desroziers et al. (2005) diagnostics help to detect and correct possible imbalances between the error covariance matrices in a variational assimilation framework in the observational space. These diagnostics assume that both the observations and the prior control vector do not have any bias. This assumption does not necessarily hold for all the experiments in this work, so we decided not to inflate the covariance matrices. Additionally, a common configuration for all the inversions is fairer to draw consistent conclusions across the five observational datasets.

The number of assimilated observations (once reprojected onto the model grid) is considerably larger than the ones used in EBCH16 due to the inclusion of fine AOD. The number of assimilated observations is 1,469,252 for MODIS/Aqua, 1,486,774 for MODIS/Terra, 906,949 for PARASOL, 385,638 for MISR, and 1,299,764 for SEVIRI. As discussed previously the differ-

Atmos. Chem. Phys. Discuss., doi:10.5194/acp-2016-1011, 2017
Manuscript under review for journal Atmos. Chem. Phys.
Discussion started: 10 February 2017




ences for the instruments onboard sun-synchronous orbit satellites arise from the swath of the instruments, the amount of land retrievals, and details of the cloud masking algorithm that may reject more or less satellite pixels during the retrieval.

We compute the analysis with the assimilation system described below for five satellite retrievals dataset (MODIS/Aqua, MODIS/Terra, MISR, PARASOL and SEVIRI) for the year 2006. The assimilated observations are total AOD and fine AOD where it is available, that is, total AOD over ocean for all the retrievals; total AOD over land for MODIS, MISR and SEVIRI retrieval; fine AOD over ocean for MODIS, MISR and PARASOL; and fine AOD over land for PARASOL and MISR datasets. For satellites in the "A-Train" (MODIS/Aqua and PARASOL) the sampling is done at 13:30 local time. For instruments onboard the Terra satellite (MISR, MODIS/Terra) the sampling is done at 10:30 local time. For SEVIRI, the whole day average is considered. Only observations between 70°W and 65°E in longitude and between 0°N and 40°N in latitude are assimilated.

It is necessary to note that the fine AOD derived from the satellite observations is comparable to the model fine mode AOD but there are small differences across instruments. For MODIS and PARASOL products, the fine AOD is the contribution of preselected fine mode aerosol models to the total AOD in their respective retrieval algorithms, and they are comparable (but not necessarily equivalent) to the LMDZ-SPLA fine mode AOD. For fine AOD from MISR, our post-processing of the MISR products ensures the equivalence and comparability between the model and the assimilated fine mode AOD.

As a consequence of the structure of the control vector, where fine and coarse dust correction factors are lumped together, the assimilated fine AOD partially constrains the coarse dust correction factor. In contrast the super coarse dust correction factors are solely directly constrained by the Total dust AOD. Finally, the nonzero covariances between errors of both dust correction factors propagate the assimilation of the fine mode AOD to the super-coarse dust correction factor.

## 3 Results

### 3.1 Some words about the observations

Figure 1 shows the annual average for year 2006 of the observations described in Sect. 2.3. Several characteristics can be identified in these yearly averages of AOD and they will impact the assimilation analysis. All panels clearly show the transatlantic dust plume and the local maximum of AOD in the south of the Red Sea. However, maximum values of AOD over and downwind Bodélé depression are hardly shown in the SEVIRI and PARASOL observations. For total AOD, the SEVIRI plume over the Atlantic seems to be more extended than the rest of the products. Maximum values of total AOD over the Atlantic ocean are found close the African coast except for SEVIRI. MODIS retrievals share similar yearly AOD means for fine AOD and total AOD. In comparison, MISR AOD shows a local maximum of AOD close to (18°N, 5°W) that is not observed in the rest of the products, while an AOD local maximum at (12°N, 9°E) is only observed in the MODIS products.

For the fine AOD there are notorious differences between PARASOL and MISR products, especially over the Sahara. PARASOL AODs are significantly smaller than MISR fine mode AOD over land and ocean.

To (roughly) be able to discriminate the effect of the satellite coverage against the effect of the sampling time of the assimilated products, we have computed an equivalent of Fig. 1 but only for pairs of simultaneous AOD retrievals that correspond to (approximately) the same overpass time. These yearly averages are shown in Fig. 2. In Fig. 2 the observations of two in-

Atmos. Chem. Phys. Discuss., doi:10.5194/acp-2016-1011, 2017
Manuscript under review for journal Atmos. Chem. Phys.
Discussion started: 10 February 2017


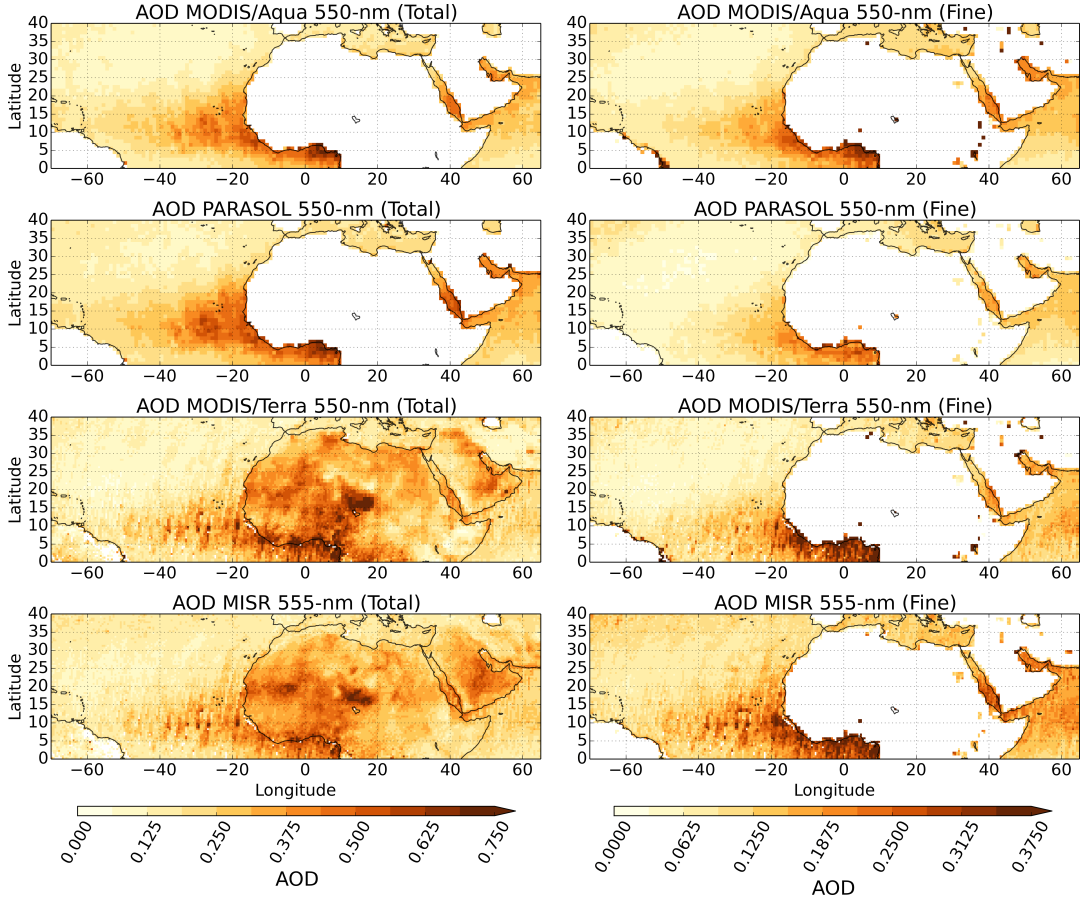


**Figure 2.** Averages for the year 2006 of the satellite-derived AOD products, similar to Fig. 1 but for colocated MISR and MODIS/Terra observations, and colocated PARASOL and MODIS/Aqua observations.

struments onboard the Terra satellite (MISR and MODIS/Terra) were screened in order to compute the yearly average with pixels where both MISR and MODIS/Terra report valid data. A similar procedure was applied to the instruments onboard satellites of the A-train constellation, MODIS/Aqua and PARASOL. This screening allows a fair comparison between two pairs of retrievals.

For the collocated averages over the ocean, MODIS/Aqua and PARASOL show a similar spatial pattern for the total AOD, with collocated maxima of AOD over the Atlantic Ocean in the 5 to 15°N latitude band; both share a relative large AOD over the Gulf of Guinea and the AOD gradient in the Red Sea (with larger values in the south of the Sea). However total AOD from MODIS/Aqua panel in Fig. 2 is slightly smaller than its PARASOL counterpart on the eastern transatlantic dust plume, while for the fine mode AOD, PARASOL shows smaller values.

Atmos. Chem. Phys. Discuss., doi:10.5194/acp-2016-1011, 2017
Manuscript under review for journal Atmos. Chem. Phys.
Discussion started: 10 February 2017


Atmospheric Chemistry and Physics Discussions

For MODIS/Terra and MISR the differences mentioned in the description of Fig. 1 still holds when the observations are collocated (Fig. 2). Over the Arabian Peninsula, a spatial mismatch between MODIS products and MISR AOD can be identified in both Fig. 1 and Fig. 2.

### 3.2 Assimilation results: Departures

The assimilation performance will be explained only in terms of observation departures. Comparisons with the assimilated AOD are qualitatively similar to those presented in EBCH16.

Figure 3 shows histograms (in 200 bins) of the departures of the prior AOD (i.e., the difference between assimilated observations and the simulated prior AOD) and the departures of the analysis (i.e., the difference between the assimilated observations and the analysis AOD). This is shown for all 5 experiments. A common and expected feature of Fig. 3 is the smaller dispersion of the analysis departures with respect to the prior ones. The mode value of the histogram of the departures for the analysis is also closer to zero than for the prior in all the panels for the total AOD.

All prior histograms except PARASOL, are slightly shifted to the right instead of being centered on zero, which means that the observations are generally larger than the prior, or said differently that the model has a low bias. This is repeated to a lesser extent in the analysis histograms for MODIS/Terra, MODIS/Aqua and MISR. For these three instruments, the land and ocean departures of the total AOD share similar characteristics, that is, ocean departures have less spread than land departures, and the right tails of land departures are heavier than their ocean counterpart.

We recall that the prior simulation is the same for all panels, and the difference in prior lies in the local time and gridboxes for which the model values are sampled. Despite the sampling difference and given the differences between the collocated AODs (above explained) we nevertheless think that most differences between the histograms of Fig. 3 are due to observational differences.

The only instrument that does not have available total AOD over land is the PARASOL instrument. Departures of total AOD over ocean are larger in the PARASOL panel than for the rest of the satellites, with a notable shift to the right, meaning that the observations are, in most of the cases, larger than the prior and analysis simulations. These large departures in the prior are mostly related to the large AOD values of the dust transatlantic plume over the Eastern Atlantic Ocean.

Validation against Aerosol Robotic Network (AERONET Holben et al., 1998) is qualitatively similar to the one shown in EBCH16 for all the experiments. A table summarizing the main statistics for each experiment is included in Appendix A.

### 3.3 Analysis AOD

Figure 4 shows the simulated 550 $\mathrm{nm}$ AOD for the prior and the 5 analyses. Larger AOD values are simulated in boreal summer (June-July-August or JJA) for all the analysis and the prior. Compared to the prior, the analysis decreases AOD in the northern Sahara for all the analysis except PARASOL in JJA and boreal spring (March-April-May or MAM). There is not a large difference in AOD when the two MODIS analyses are compared between them, which is consistent with the discussion of the observations in Sect. 3.1. AOD from the MISR assimilation is larger in MAM than in the MODIS analysis.

Atmos. Chem. Phys. Discuss., doi:10.5194/acp-2016-1011, 2017
Manuscript under review for journal Atmos. Chem. Phys.
Discussion started: 10 February 2017


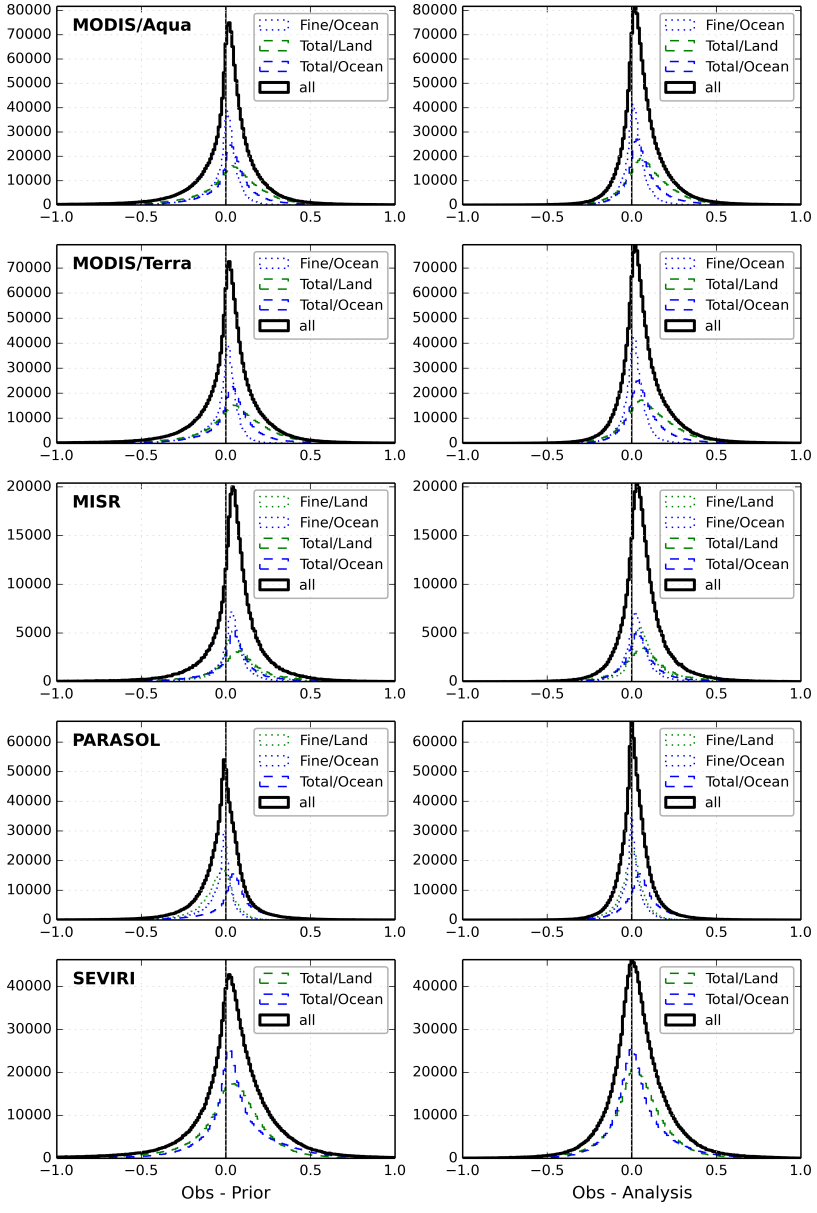


**Figure 3.** Frequency plot of departures. Observational departures with respect to the prior simulation are shown on the left column and departures with respect to the analysis are shown on the right column. Histograms are plotted between -1 and 1 in 200 bins each. Pixels over land are in green, over ocean in blue and both of them in black. Fine mode AOD in dotted lines and Total AOD in dashed lines.

In the PARASOL analysis the assimilation system increases the coarser dust emissions in order to improve the fit over the ocean. As PARASOL does not report total AOD over land, dust emissions of the coarser dust bins (and thus also with the

Atmos. Chem. Phys. Discuss., doi:10.5194/acp-2016-1011, 2017
Manuscript under review for journal Atmos. Chem. Phys.
Discussion started: 10 February 2017


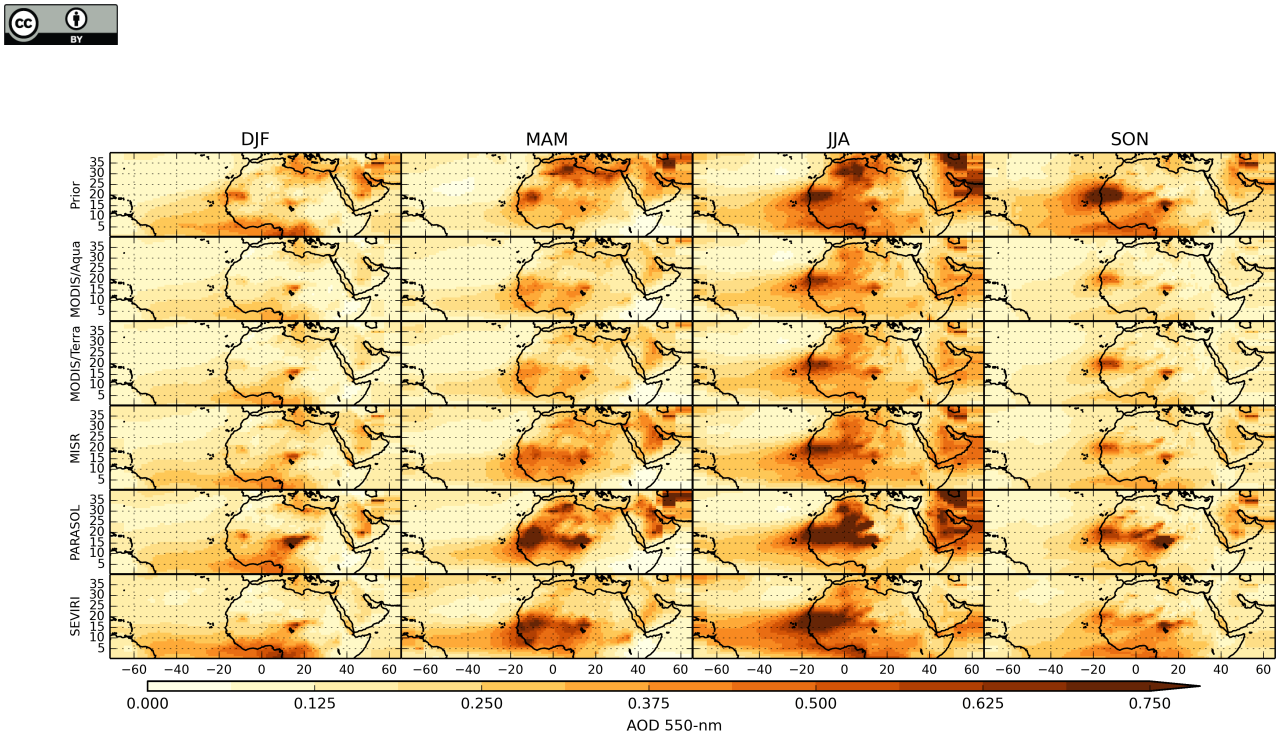


**Figure 4.** Simulated prior and analysis AOD at 550 nm for the 5 assimilation configurations. The panels show the averaged AOD for each experiment (rows) over the months indicated in the head of the columns. MAM stands for March, April and May; JJA for June, July and August, SON for September, October and November and DJF for December, January and February. In the later we include the first two months and the last month of the year 2006.

shorter atmospheric residence time) are not fully constrained by near-source observations. This results in a large and possible unrealistic increase in coarser mode dust emissions. For this reason we exclude this dataset from our emission flux analysis.

The SEVIRI analysis shows a larger transatlantic dust plume in MAM and JJA along with larger values of AOD over land. Observational uncertainties for SEVIRI are generally larger over land than over ocean. This allows the assimilation system to favour a better fit of the AOD over the ocean than over land, which results in large AOD values over land.

The relatively large AOD over land of the last two analyses (PARASOL and SEVIRI) could indicate a deficiency in the model in the transport of the dust plume. We will come back to this point later in this work.

### 3.4 Mineral dust flux

Mineral dust emissions were estimated with the data assimilation system using the five satellite products one by one. Total estimated flux over the Sahara and the Arabian Peninsula are shown in Table 2. Excluding the PARASOL analysis, the total mineral dust fluxes for the year 2006 ranges between 2547 and 3680 Tg. We recall that these estimates are for emitted dust particles in a diameter range between 0.06 and 30 µm. The emission estimate is highly dependent on the size cut-off of the emitted particles. For airborne dust smaller than 6 µm of diameter, the total flux is estimated between 630 and 853 Tg for the year 2006. The range is therefore much smaller when we exclude the largest dust mode. Table 2 shows detailed estimates for these categories and for three geographical regions: Western North Africa, Eastern North Africa and the Arabian Peninsula.

Atmos. Chem. Phys. Discuss., doi:10.5194/acp-2016-1011, 2017
Manuscript under review for journal Atmos. Chem. Phys.
Discussion started: 10 February 2017


Atmospheric Chemistry and Physics Discussions

**Table 2.** Total emission flux by region and by observational dataset for the year 2006 in $\mathrm{Tg\ year^{-1}}$. AP stands for Arabian Peninsula. Western Africa refers to the longitude band between the Atlantic coast and approximately 16°E corresponding to regions 01 to 09 in EBCH16. East Africa refers to regions 10 to 16 in EBCH16, that is, to a longitude band between approximately 16°E and the Red Sea.

| | Prior | MODIS/Terra | MODIS/Aqua | MISR | PARASOL | SEVIRI |
|---|---|---|---|---|---|---|
| Total AP+Africa | 6657 | 3267 | 2697 | 3680 | 15748 | 2547 |
| Total Africa | 4085 | 2788 | 2361 | 2638 | 9447 | 2404 |
| Total AP | 2571 | 478 | 337 | 1043 | 6301 | 143 |
| Total Africa West | 3161 | 1808 | 1484 | 1699 | 6672 | 1544 |
| Total Africa East | 924 | 980 | 877 | 938 | 2775 | 860 |
| Fine and Coarse AP+Africa | 1087 | 644 | 630 | 853 | 874 | 670 |
| Fine and Coarse Africa | 709 | 452 | 431 | 585 | 527 | 567 |
| Fine and Coarse AP | 378 | 192 | 199 | 268 | 347 | 103 |
| Fine and Coarse Africa West | 526 | 294 | 290 | 376 | 357 | 379 |
| Fine and Coarse Africa East | 183 | 158 | 141 | 209 | 170 | 188 |
| Super-coarse AP+Africa | 5570 | 2623 | 2067 | 2827 | 14873 | 1877 |
| Super-coarse Africa | 3376 | 2336 | 1930 | 2052 | 8920 | 1837 |
| Super-coarse AP | 2193 | 287 | 138 | 775 | 5954 | 39 |
| Super-coarse Africa West | 2635 | 1514 | 1194 | 1324 | 6314 | 1165 |
| Super-coarse Africa East | 741 | 822 | 736 | 729 | 2605 | 672 |

Similarly to the emissions presented in Laurent et al. (2008), Western Sahara has larger emissions than Eastern Sahara. This is indeed the case in all the analysis. For both fine and coarse dust emissions, the contribution of the Arabian Peninsula (AP) is significant, indicating that is an important dust source eventhough it does not receive much attention in the literature. However, super-coarse dust emissions of AP are, in general, one order of magnitude smaller than North African emissions.

Figure 5 shows emission fluxes split by month for the three bins of SPLA. It can be seen that most of the dust emission flux is achieved in the super-coarse size range. For the reasons explained above, super-coarse dust emissions of the PARASOL analysis are much larger than expected. However, this is not the case for the coarse dust flux of the PARASOL analysis due to the structure of the control vector, where the fine and coarse dust correction factors are lumped together. As it was the case in EBCH16, the dust emission fluxes from the analysis are systematically smaller than for the prior simulation, for almost all dust bins, regions and months. This is largely noticeable for the super-coarse dust emission panel.

In general, coarse and fine dust emissions have maximum values in July, June, March and December while the super-coarse dust emission peaks on September. Throughout the year, coarse and fine dust fluxes share the same emission cycle, indicating consistent seasonality across the various assimilated observational datasets. However, we cannot completely discard that a model bias (at the seasonal scale) generates this feature.

Atmos. Chem. Phys. Discuss., doi:10.5194/acp-2016-1011, 2017
Manuscript under review for journal Atmos. Chem. Phys.
Discussion started: 10 February 2017


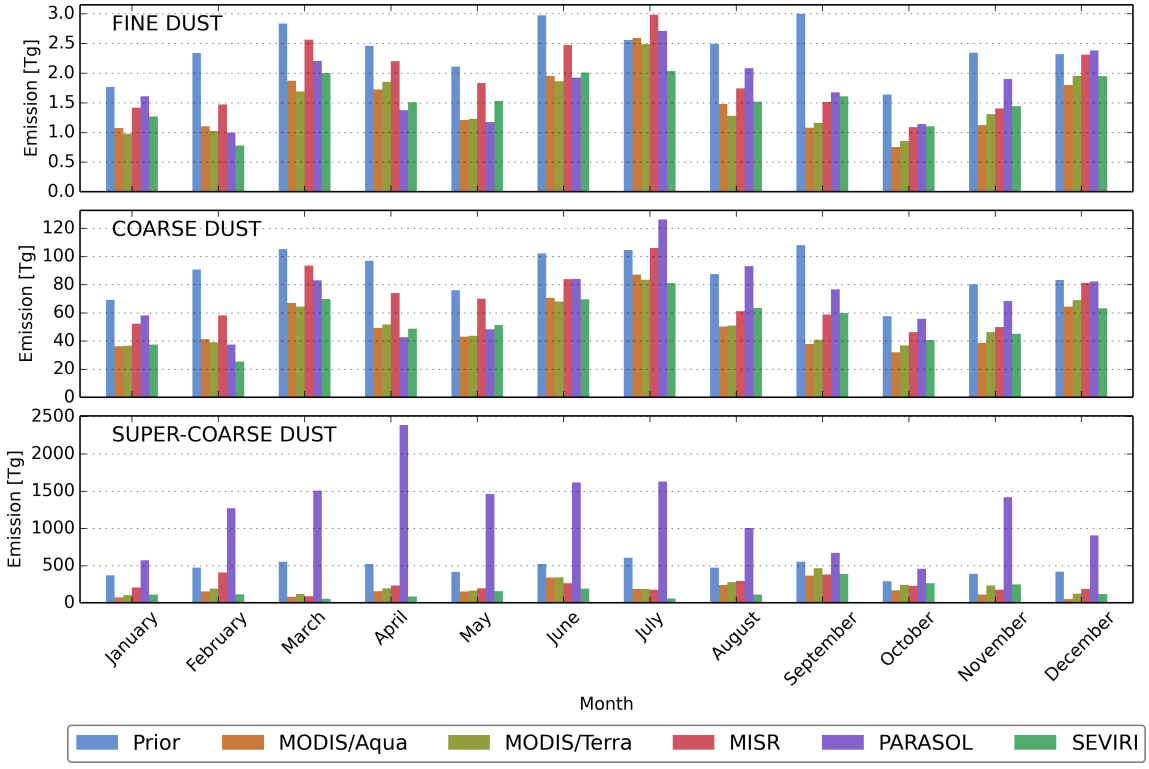


**Figure 5.** Total dust flux per month over the Sahara and the Arabian Peninsula. Fine mode dust is shown in the first panel, coarse mode dust in the middle panel and super-coarse mode dust in the lower panel. The different bars show the total mineral dust flux over the Sahara and the Arabian Peninsula by experiment and month. The three plots use different scales.

Sensitivity to the observation sampling time and coverage is not explored in this work explicitly, but the impact of the sampling time can be somehow inferred from a comparison between the two MODIS analyses. Both MODIS retrievals are expected to have similar performance when compared against reference datasets (Levy et al., 2015; Sayer et al., 2015). Our results indicate that, despite the relatively large spread (hundreds of Tg per year) on the overall analysed dust flux from the two instruments, the seasonal cycle of these two analyses is similar.

If both instruments are unbiased (or at least if they have the same bias), the sampling time of the products would be the most important difference in the data assimilation system. In this case, the mismatch on the overall emission flux, which is controlled by emissions from the super-coarse dust, can be likely attributed to the representation of the diurnal cycle of model emissions and boundary layer processes.

Atmos. Chem. Phys. Discuss., doi:10.5194/acp-2016-1011, 2017
Manuscript under review for journal Atmos. Chem. Phys.
Discussion started: 10 February 2017


Atmospheric Chemistry and Physics Discussions

## 4 Conclusions

We have assimilated AOD from five satellite retrievals into a common data assimilation system. The control vector elements consist of correction factors for the prior aerosol emission flux over sub-regions of the Sahara and the Arabian Peninsula. Observational error statistics were adapted from the literature. For four of the five AOD datasets fine mode AOD was assimilated when it was available. As expected, the analysis departures are, in general, smaller than the prior departures. The a posteriori estimated mineral dust flux shares a common seasonal variation between the various data assimilation configurations, but there is a relative large spread in the yearly total amount. This work estimates a total amount of emitted mineral dust over North Africa and the Arabian Peninsula ranging between 2550 and 3680 $\mathrm{Tg\,yr^{-1}}$, for mineral dust particles smaller than 30 $\mu\mathrm{m}$ of diameter in the year 2006. For mineral dust smaller than 6 $\mu\mathrm{m}$ of diameter, the estimated flux is between 630 and 850 $\mathrm{Tg\,yr^{-1}}$.

We isolated the role of the assimilated observation dataset (by freezing the rest of the inversion configuration) and showed that the large spread of these fluxes is likely associated to differences between these datasets (including their associated error statistics) rather than to model biases or deficiencies in the data assimilation system. This is despite the satellite AOD observations being similarly good quality (or at least perceived as such). The dust emission fluxes are nevertheless sensitive to model biases or missing or under-represented processes in the model. In fact, the large emission of super-coarse dust in the PARASOL experiment could indicate that the model is not able to well reproduce airborne dust transport and removal processes. For this product, a coarse AOD retrieval over land would be beneficial in the assimilation.

Despite the fact that MISR has a smaller swath compared to the other assimilated products, the capability of report total and fine AOD over land is beneficial to the assimilation. This can be seen when the analysis was compared against AERONET AOD (Appendix A), the MISR analysis skills are similar to the rest of the analyses although the number of assimilated observations is smaller.

It is important to maintain the variety of current AOD retrieval approaches, explored by different groups with different algorithms, while improving the quality and achieving some convergence (through error reduction of the individual products). There are however two limitations in our treatment of observational errors due to the lack of information about the assimilated products. First, the assimilated fine AOD error variance was assumed to be similar to the total AOD error variance. Indeed, the characteristics of fine AOD errors are unknown, but this information would be useful and could, in principle, improve the analysis. Secondly, we assumed uncorrelated errors between fine and total assimilated AOD. As both AODs are computed simultaneously in the retrievals using similar hypotheses and radiance measurements, this assumption does not necessarily hold. Ideally, these statistics should be provided by the retrieval algorithm and reported along with the observations. Likewise it would be useful to consider error covariances in space (and possibly in time). A new generation of aerosol retrieval algorithms based on statistically optimized fitting of observations, such as that of GRASP (Dubovik et al., 2014), can in principle provide such information. It would be interesting to test the impact of including such improved error statistics in the source inversion.

The year-to-year variability of dust emission fluxes was not considered in this study. It could increase or decrease the spread in dust emission fluxes estimates. Although different satellite aerosol instruments are available for different periods, there are sufficient overlaps between instruments to gain understanding from multi-year retrievals.

Atmos. Chem. Phys. Discuss., doi:10.5194/acp-2016-1011, 2017
Manuscript under review for journal Atmos. Chem. Phys.
Discussion started: 10 February 2017


Atmospheric Chemistry and Physics Discussions

| Station | | Bahrain | Blida | Dhabi | Dhadnah | Forth Crete | Granada | Hamim | Ilorin | La Parguera | Nes Ziona | Santa Cruz Tenerife | Sede Boker | Solar Village |
|---|---|---|---|---|---|---|---|---|---|---|---|---|---|---|
| Latitude (°N) | | 26.21 | 36.51 | 24.48 | 25.51 | 35.33 | 37.16 | 22.97 | 8.32 | 17.97 | 31.92 | 28.47 | 30.86 | 24.91 |
| Longitude (°E) | | 50.61 | 2.88 | 54.38 | 56.32 | 25.28 | -3.6 | 54.3 | 4.34 | -67.05 | 34.79 | -16.25 | 34.78 | 46.4 |
| Elevation (m.a.s.l.) | | 25 | 230 | 15 | 81 | 20 | 680 | 209 | 350 | 12 | 40 | 52 | 480 | 764 |
| N obs. | | 201 | 195 | 243 | 324 | 283 | 276 | 263 | 270 | 251 | 185 | 233 | 335 | 335 |
| Mean | Obs. | 0.433 | 0.258 | 0.434 | 0.404 | 0.196 | 0.177 | 0.314 | 0.705 | 0.148 | 0.226 | 0.171 | 0.2 | 0.372 |
| | Prior | 0.472 | 0.313 | 0.411 | 0.454 | 0.273 | 0.209 | 0.346 | 0.434 | 0.145 | 0.245 | 0.178 | 0.263 | 0.37 |
| | MODIS/Aqua | 0.304 | 0.179 | 0.236 | 0.242 | 0.176 | 0.127 | 0.196 | 0.319 | 0.113 | 0.14 | 0.119 | 0.168 | 0.276 |
| | MODIS/Terra | 0.309 | 0.187 | 0.238 | 0.241 | 0.184 | 0.133 | 0.196 | 0.329 | 0.116 | 0.151 | 0.126 | 0.187 | 0.289 |
| | MISR | 0.429 | 0.216 | 0.321 | 0.326 | 0.221 | 0.161 | 0.262 | 0.392 | 0.135 | 0.198 | 0.146 | 0.274 | 0.383 |
| | PARASOL | 0.452 | 0.197 | 0.349 | 0.372 | 0.166 | 0.129 | 0.286 | 0.379 | 0.109 | 0.141 | 0.138 | 0.204 | 0.449 |
| | SEVIRI | 0.267 | 0.22 | 0.208 | 0.203 | 0.222 | 0.173 | 0.188 | 0.487 | 0.194 | 0.192 | 0.166 | 0.219 | 0.267 |
| Bias | Prior | 0.04 | 0.056 | -0.023 | 0.05 | 0.076 | 0.032 | 0.032 | -0.271 | -0.003 | 0.019 | 0.007 | 0.063 | -0.002 |
| | MODIS/Aqua | -0.128 | -0.079 | -0.198 | -0.162 | -0.02 | -0.05 | -0.118 | -0.386 | -0.035 | -0.085 | -0.052 | -0.031 | -0.097 |
| | MODIS/Terra | -0.123 | -0.071 | -0.196 | -0.163 | -0.012 | -0.044 | -0.118 | -0.376 | -0.032 | -0.075 | -0.045 | -0.013 | -0.083 |
| | MISR | -0.003 | -0.041 | -0.113 | -0.078 | 0.024 | -0.016 | -0.053 | -0.313 | -0.013 | -0.028 | -0.025 | 0.074 | 0.011 |
| | PARASOL | 0.019 | -0.061 | -0.085 | -0.032 | -0.031 | -0.048 | -0.028 | -0.326 | -0.039 | -0.085 | -0.033 | 0.004 | 0.077 |
| | SEVIRI | -0.165 | -0.038 | -0.226 | -0.201 | 0.026 | -0.004 | -0.126 | -0.218 | 0.046 | -0.034 | -0.005 | 0.019 | -0.105 |
| RMSE | Prior | 0.365 | 0.349 | 0.397 | 0.465 | 0.266 | 0.229 | 0.257 | 0.598 | 0.146 | 0.144 | 0.176 | 0.235 | 0.272 |
| | MODIS/Aqua | 0.264 | 0.172 | 0.306 | 0.28 | 0.143 | 0.109 | 0.191 | 0.607 | 0.087 | 0.142 | 0.112 | 0.129 | 0.264 |
| | MODIS/Terra | 0.258 | 0.167 | 0.307 | 0.28 | 0.145 | 0.108 | 0.193 | 0.604 | 0.086 | 0.14 | 0.109 | 0.155 | 0.258 |
| | MISR | 0.366 | 0.186 | 0.283 | 0.276 | 0.176 | 0.127 | 0.178 | 0.564 | 0.086 | 0.138 | 0.106 | 0.576 | 0.269 |
| | PARASOL | 0.381 | 0.21 | 0.295 | 0.286 | 0.158 | 0.144 | 0.226 | 0.566 | 0.094 | 0.152 | 0.112 | 0.294 | 0.478 |
| | SEVIRI | 0.273 | 0.156 | 0.329 | 0.288 | 0.155 | 0.113 | 0.205 | 0.518 | 0.11 | 0.132 | 0.1 | 0.188 | 0.261 |
| $\rho$ | Prior | 0.256 | 0.572 | 0.232 | 0.147 | 0.367 | 0.658 | 0.454 | 0.086 | 0.284 | 0.464 | 0.396 | 0.546 | 0.393 |
| | MODIS/Aqua | 0.465 | 0.67 | 0.384 | 0.307 | 0.379 | 0.716 | 0.589 | 0.439 | 0.465 | 0.463 | 0.665 | 0.532 | 0.452 |
| | MODIS/Terra | 0.468 | 0.685 | 0.357 | 0.28 | 0.393 | 0.718 | 0.569 | 0.432 | 0.458 | 0.447 | 0.669 | 0.496 | 0.472 |
| | MISR | 0.352 | 0.632 | 0.355 | 0.29 | 0.423 | 0.702 | 0.539 | 0.436 | 0.406 | 0.434 | 0.649 | 0.556 | 0.43 |
| | PARASOL | 0.274 | 0.635 | 0.374 | 0.308 | 0.403 | 0.676 | 0.537 | 0.434 | 0.406 | 0.431 | 0.647 | 0.382 | 0.205 |
| | SEVIRI | 0.486 | 0.676 | 0.286 | 0.348 | 0.415 | 0.681 | 0.495 | 0.406 | 0.461 | 0.43 | 0.683 | 0.274 | 0.484 |

**Table A1.** Statistics of the analyses against AERONET 500-nm AOD for selected sites. The acronym m.a.s.l. stands for meters above sea level, RMSE for root mean square error and $\rho$ is the Pearson correlation coeficient.

Finally reducing modelled and observational biases is another key to improve top-down emission flux estimates. Pope et al. (2016) evaluated the analysis increments in a data assimilation framework and found that large increments were associated with meteorological conditions for which the model lacks performance. Another approach which we leave for future work would be to optimize some of key model parameters in the dust source function.

## Appendix A: Comparison with AERONET

For validation, we select AERONET stations in the same way as in EBCH16. We only consider stations with at least 182 valid daily 500 nm AOD retrievals of Level 2 product (Version 2). The following stations meet this criteria for the year 2006 in the region of interest: Bahrain, Blida, Dhabi, Dhadnah, Forth Crete, Granada, Hamim, Ilorin, La Parguera, Nes Ziona, Santa Cruz Tenerife, Sede Boker and Solar Village. The model AOD is recomputed at 500 nm for comparison with the AERONET AOD. The summary of statistics is shown in Table A1.

*Competing interests.* The authors declare that they have no conflict of interest.

*Acknowledgements.* The authors would like to thank the MODIS, MISR, PARASOL, AERUS-GEO and AERONET teams for making their retrieval available, F.-M. Bréon and D. Carrer for their advice with the POLDER/PARASOL and the AERUS-GEO retrievals, respectively. The POLDER/PARASOL and AERUS-GEO data were downloaded from the ICARE analysis and data centre (http://www.icare.univ-lille1.fr/). MODIS AOD products are available at http://modis-atmos.gsfc.nasa.gov, MISR AOD were downloaded from the Atmospheric Science Data Center at NASA (https://eosweb.larc.nasa.gov/) and AERONET AOD is available at http://aeronet.gsfc.nasa.gov. Input soil data used in this study is available at http://www.lisa.univ-paris12.fr/mod/data/index.php. The work was co-funded by the project OSIRIS from MEDDE/INSU, the Copernicus Atmosphere Monitoring Service, implemented by the European Centre for Medium-Range Weather Forecasts (ECMWF) on behalf of the European Commission, and by the France-Chile ECOS project number C14U01. Part of the work was done using computing time from the TGCC under the GENCI projects t2014012201, t2015012201 and t2016012201. Nicolás Huneeus acknowledges support from FONDAP 15110009 and FONDECYT 1150873.



## References

Alfaro, S. C. and Gomes, L.: Modeling mineral aerosol production by wind erosion: Emission intensities and aerosol size distributions in source areas, Journal of Geophysical Research: Atmospheres, 106, 18 075–18 084, doi:10.1029/2000JD900339, http://dx.doi.org/10.1029/2000JD900339, 2001.

Benedetti, A., Morcrette, J.-J., Boucher, O., Dethof, A., Engelen, R. J., Fisher, M., Flentje, H., Huneeus, N., Jones, L., Kaiser, J. W., Kinne, S., Mangold, A., Razinger, M., Simmons, A. J., and Suttie, M.: Aerosol analysis and forecast in the European Centre for Medium–Range Weather Forecasts Integrated Forecast System: 2. Data assimilation, Journal of Geophysical Research: Atmospheres, 114, doi:10.1029/2008JD011115, http://dx.doi.org/10.1029/2008JD011115, d13205, 2009.

Bond, T. C., Doherty, S. J., Fahey, D. W., Forster, P. M., Berntsen, T., DeAngelo, B. J., Flanner, M. G., Ghan, S., Kärcher, B., Koch, D., Kinne, S., Kondo, Y., Quinn, P. K., Sarofim, M. C., Schultz, M. G., Schulz, M., Venkataraman, C., Zhang, H., Zhang, S., Bellouin, N., Guttikunda, S. K., Hopke, P. K., Jacobson, M. Z., Kaiser, J. W., Klimont, Z., Lohmann, U., Schwarz, J. P., Shindell, D., Storelvmo, T., Warren, S. G., and Zender, C. S.: Bounding the role of black carbon in the climate system: A scientific assessment, Journal of Geophysical Research: Atmospheres, 118, 5380–5552, doi:10.1002/jgrd.50171, http://dx.doi.org/10.1002/jgrd.50171, 2013.

Carrer, D., Roujean, J.-L., Hautecoeur, O., and Elias, T.: Daily estimates of aerosol optical thickness over land surface based on a directional and temporal analysis of SEVIRI MSG visible observations, Journal of Geophysical Research: Atmospheres, 115, doi:10.1029/2009JD012272, http://dx.doi.org/10.1029/2009JD012272, d10208, 2010.

Carrer, D., Ceamanos, X., Six, B., and Roujean, J.-L.: AERUS-GEO: A newly available satellite-derived aerosol optical depth product over Europe and Africa, Geophysical Research Letters, 41, 7731–7738, doi:10.1002/2014GL061707, http://dx.doi.org/10.1002/2014GL061707, 2014.

de Leeuw, G., Holzer-Popp, T., Bevan, S., Davies, W. H., Descloitres, J., Grainger, R. G., Griesfeller, J., Heckel, A., Kinne, S., Klüser, L., Kolmonen, P., Litvinov, P., Martynenko, D., North, P., Ovigneur, B., Pascal, N., Poulsen, C., Ramon, D., Schulz, M., Siddans, R., Sogacheva, L., Tanré, D., Thomas, G. E., Virtanen, T. H., von Hoyningen Huene, W., Vountas, M., and Pinnock, S.: Evaluation of seven European aerosol optical depth retrieval algorithms for climate analysis, Remote Sensing of Environment, 162, 295 – 315, doi:http://dx.doi.org/10.1016/j.rse.2013.04.023, http://www.sciencedirect.com/science/article/pii/S0034425713003507, 2015.

Dee, D. P., Uppala, S. M., Simmons, A. J., Berrisford, P., Poli, P., Kobayashi, S., Andrae, U., Balmaseda, M. A., Balsamo, G., Bauer, P., Bechtold, P., Beljaars, A. C. M., van de Berg, L., Bidlot, J., Bormann, N., Delsol, C., Dragani, R., Fuentes, M., Geer, A. J., Haimberger, L., Healy, S. B., Hersbach, H., Hólm, E. V., Isaksen, L, Kållberg, P., Köhler, M., Matricardi, M., McNally, A. P., Monge-Sanz, B. M., Morcrette, J.-J., Park, B.-K., Peubey, C., de Rosnay, P., Tavolato, C., Thépaut, J.-N., and Vitart, F.: The ERA–Interim reanalysis: configuration and performance of the data assimilation system, Quarterly Journal of the Royal Meteorological Society, 137, 553–597, doi:10.1002/qj.828, http://dx.doi.org/10.1002/qj.828, 2011.

Desroziers, G., Berre, L., Chapnik, B., and Poli, P.: Diagnosis of observation, background and analysis–error statistics in observation space, Quarterly Journal of the Royal Meteorological Society, 131, 3385–3396, doi:10.1256/qj.05.108, http://dx.doi.org/10.1256/qj.05.108, 2005.

Dubovik, O., Lapyonok, T., Kaufman, Y. J., Chin, M., Ginoux, P., Kahn, R. A., and Sinyuk, A.: Retrieving global aerosol sources from satellites using inverse modeling, Atmospheric Chemistry and Physics, 8, 209–250, doi:10.5194/acp-8-209-2008, http://www.atmos-chem-phys.net/8/209/2008/, 2008.

Dubovik, O., Lapyonok, T., Litvinov, P., Herman, M., Fuertes, D., Ducos, F., Lopatin, A., Chaikovsky, A., Torres, B., Derimian, Y., et al.: GRASP: a versatile algorithm for characterizing the atmosphere, SPIE: Newsroom, doi:10.1117/2.1201408.005558, http://spie.org/newsroom/5558-grasp-a-versatile-algorithm-for-characterizing-the-atmosphere/, 2014.

Escribano, J., Boucher, O., Chevallier, F., and Huneeus, N.: Subregional inversion of North African dust sources, Journal of Geophysical Research: Atmospheres, 121, 8549–8566, doi:10.1002/2016JD025020, http://dx.doi.org/10.1002/2016JD025020, 2016JD025020, 2016.

Evan, A. T., Flamant, C., Fiedler, S., and Doherty, O.: An analysis of aeolian dust in climate models, Geophysical Research Letters, 41, 5996–6001, doi:10.1002/2014GL060545, http://dx.doi.org/10.1002/2014GL060545, 2014GL060545, 2014.

Holben, B., Eck, T., Slutsker, I., Tanré, D., Buis, J., Setzer, A., Vermote, E., Reagan, J., Kaufman, Y., Nakajima, T., Lavenu, F., Jankowiak, I., and Smirnov, A.: AERONET–A Federated Instrument Network and Data Archive for Aerosol Characterization, Remote Sensing of Environment, 66, 1 – 16, doi:http://dx.doi.org/10.1016/S0034-4257(98)00031-5, http://www.sciencedirect.com/science/article/pii/S0034425798000315, 1998.

Hourdin, F., Grandpeix, J.-Y., Rio, Catherine a Bony, S., Jam, A., Cheruy, F., Rochetin, N., Fairhead, L., Idelkadi, A., Musat, I., Dufresne, J.-L., Lahellec, A., Lefebvre, M.-P., and Roehrig, R.: LMDZ5B: the atmospheric component of the IPSL climate model with revisited parameterizations for clouds and convection, Climate Dynamics, 40, 2193–2222, doi:10.1007/s00382-012-1343-y, http://dx.doi.org/10.1007/s00382-012-1343-y, 2013.

Huneeus, N., Boucher, O., and Chevallier, F.: Simplified aerosol modeling for variational data assimilation, Geoscientific Model Development, 2, 213–229, doi:10.5194/gmd-2-213-2009, http://www.geosci-model-dev.net/2/213/2009/, 2009.

Huneeus, N., Schulz, M., Balkanski, Y., Griesfeller, J., Prospero, J., Kinne, S., Bauer, S., Boucher, O., Chin, M., Dentener, F., Diehl, T., Easter, R., Fillmore, D., Ghan, S., Ginoux, P., Grini, A., Horowitz, L., Koch, D., Krol, M. C., Landing, W., Liu, X., Mahowald, N., Miller, R., Morcrette, J.-J., Myhre, G., Penner, J., Perlwitz, J., Stier, P., Takemura, T., and Zender, C. S.: Global dust model intercomparison in AeroCom phase I, Atmospheric Chemistry and Physics, 11, 7781–7816, doi:10.5194/acp-11-7781-2011, http://www.atmos-chem-phys.net/11/7781/2011/, 2011.

Huneeus, N., Chevallier, F., and Boucher, O.: Estimating aerosol emissions by assimilating observed aerosol optical depth in a global aerosol model, Atmospheric Chemistry and Physics, 12, 4585–4606, doi:10.5194/acp-12-4585-2012, http://www.atmos-chem-phys.net/12/4585/2012/, 2012.

Kahn, R., Nelson, D., Garay, M., Levy, R., Bull, M., Diner, D., Martonchik, J., Paradise, S., Hansen, E., and Remer, L.: MISR Aerosol Product Attributes and Statistical Comparisons With MODIS, Geoscience and Remote Sensing, IEEE Transactions on, 47, 4095–4114, doi:10.1109/TGRS.2009.2023115, 2009.

Kahn, R. A., Gaitley, B. J., Martonchik, J. V., Diner, D. J., Crean, K. A., and Holben, B.: Multiangle Imaging Spectroradiometer (MISR) global aerosol optical depth validation based on 2 years of coincident Aerosol Robotic Network (AERONET) observations, Journal of Geophysical Research: Atmospheres, 110, doi:10.1029/2004JD004706, http://dx.doi.org/10.1029/2004JD004706, d10S04, 2005.

Laurent, B., Marticorena, B., Bergametti, G., Léon, J. F., and Mahowald, N. M.: Modeling mineral dust emissions from the Sahara desert using new surface properties and soil database, Journal of Geophysical Research: Atmospheres, 113, doi:10.1029/2007JD009484, http://dx.doi.org/10.1029/2007JD009484, d14218, 2008.

Levy, R. C., Remer, L. A., Tanré, D., Kaufman, Y. J., Ichoku, C., Holben, B. N., Livingston, J. M., Russell, P. B., and Maring, H.: Evaluation of the Moderate-Resolution Imaging Spectroradiometer (MODIS) retrievals of dust aerosol over the ocean during PRIDE, Journal of Geophysical Research: Atmospheres, 108, doi:10.1029/2002JD002460, http://dx.doi.org/10.1029/2002JD002460, 8594, 2003.

Levy, R. C., Remer, L. A., Kleidman, R. G., Mattoo, S., Ichoku, C., Kahn, R., and Eck, T. F.: Global evaluation of the Collection 5 MODIS dark-target aerosol products over land, Atmospheric Chemistry and Physics, 10, 10 399–10 420, doi:10.5194/acp-10-10399-2010, http://www.atmos-chem-phys.net/10/10399/2010/, 2010.

Levy, R. C., Mattoo, S., Munchak, L. A., Remer, L. A., Sayer, A. M., Patadia, F., and Hsu, N. C.: The Collection 6 MODIS aerosol products over land and ocean, Atmospheric Measurement Techniques, 6, 2989–3034, doi:10.5194/amt-6-2989-2013, http://www.atmos-meas-tech.net/6/2989/2013/, 2013.

Levy, R. C., Munchak, L. A., Mattoo, S., Patadia, F., Remer, L. A., and Holz, R. E.: Towards a long-term global aerosol optical depth record: applying a consistent aerosol retrieval algorithm to MODIS and VIIRS-observed reflectance, Atmospheric Measurement Techniques, 8, 4083–4110, doi:10.5194/amt-8-4083-2015, http://www.atmos-meas-tech.net/8/4083/2015/, 2015.

Lynch, P., Reid, J. S., Westphal, D. L., Zhang, J., Hogan, T. F., Hyer, E. J., Curtis, C. A., Hegg, D. A., Shi, Y., Campbell, J. R., Rubin, J. I., Sessions, W. R., Turk, F. J., and Walker, A. L.: An 11-year global gridded aerosol optical thickness reanalysis (v1.0) for atmospheric and climate sciences, Geoscientific Model Development, 9, 1489–1522, doi:10.5194/gmd-9-1489-2016, http://www.geosci-model-dev.net/9/1489/2016/, 2016.

Marticorena, B. and Bergametti, G.: Modeling the atmospheric dust cycle: 1. Design of a soil-derived dust emission scheme, Journal of Geophysical Research: Atmospheres, 100, 16 415–16 430, doi:10.1029/95JD00690, http://dx.doi.org/10.1029/95JD00690, 1995.

Pope, R. J., Marsham, J. H., Knippertz, P., Brooks, M. E., and Roberts, A. J.: Identifying errors in dust models from data assimilation, Geophysical Research Letters, 43, 9270–9279, doi:10.1002/2016GL070621, http://dx.doi.org/10.1002/2016GL070621, 2016GL070621, 2016.

Remer, L. A., Kaufman, Y. J., Tanré, D., Mattoo, S., Chu, D. A., Martins, J. V., Li, R.-R., Ichoku, C., Levy, R. C., Kleidman, R. G., Eck, T. F., Vermote, E., and Holben, B. N.: The MODIS Aerosol Algorithm, Products, and Validation, Journal of the Atmospheric Sciences, 62, 947–973, doi:10.1175/JAS3385.1, http://dx.doi.org/10.1175/JAS3385.1, 2005.

Remer, L. A., Kleidman, R. G., Levy, R. C., Kaufman, Y. J., Tanré, D., Mattoo, S., Martins, J. V., Ichoku, C., Koren, I., Yu, H., and Holben, B. N.: Global aerosol climatology from the MODIS satellite sensors, Journal of Geophysical Research: Atmospheres, 113, doi:10.1029/2007JD009661, http://dx.doi.org/10.1029/2007JD009661, d14S07, 2008.

Saide, P. E., Kim, J., Song, C. H., Choi, M., Cheng, Y., and Carmichael, G. R.: Assimilation of next generation geostationary aerosol optical depth retrievals to improve air quality simulations, Geophysical Research Letters, 41, 9188–9196, doi:10.1002/2014GL062089, http://dx.doi.org/10.1002/2014GL062089, 2014GL062089, 2014.

Sayer, A. M., Hsu, N. C., Bettenhausen, C., and Jeong, M.-J.: Validation and uncertainty estimates for MODIS Collection 6 "Deep Blue" aerosol data, Journal of Geophysical Research: Atmospheres, 118, 7864–7872, doi:10.1002/jgrd.50600, http://dx.doi.org/10.1002/jgrd.50600, 2013.

Sayer, A. M., Munchak, L. A., Hsu, N. C., Levy, R. C., Bettenhausen, C., and Jeong, M.-J.: MODIS Collection 6 aerosol products: Comparison between Aqua's e-Deep Blue, Dark Target, and "merged" data sets, and usage recommendations, Journal of Geophysical Research: Atmospheres, 119, 13 965–13 989, doi:10.1002/2014JD022453, http://dx.doi.org/10.1002/2014JD022453, 2014JD022453, 2014.

Sayer, A. M., Hsu, N. C., Bettenhausen, C., Jeong, M.-J., and Meister, G.: Effect of MODIS Terra radiometric calibration improvements on Collection 6 Deep Blue aerosol products: Validation and Terra/Aqua consistency, Journal of Geophysical Research: Atmospheres, 120, 12,157–12,174, doi:10.1002/2015JD023878, http://dx.doi.org/10.1002/2015JD023878, 2015JD023878, 2015.

Schutgens, N., Nakata, M., and Nakajima, T.: Estimating Aerosol Emissions by Assimilating Remote Sensing Observations into a Global Transport Model, Remote Sensing, 4, 3528–3543, doi:10.3390/rs4113528, http://www.mdpi.com/2072-4292/4/11/3528, 2012.



Tanré, D., Bréon, F. M., Deuzé, J. L., Dubovik, O., Ducos, F., François, P., Goloub, P., Herman, M., Lifermann, A., and Waquet, F.: Remote sensing of aerosols by using polarized, directional and spectral measurements within the A–Train: the PARASOL mission, Atmospheric Measurement Techniques, 4, 1383–1395, doi:10.5194/amt-4-1383-2011, http://www.atmos-meas-tech.net/4/1383/2011/, 2011.

Wang, R., Balkanski, Y., Bopp, L., Aumont, O., Boucher, O., Ciais, P., Gehlen, M., Peñuelas, J., Ethé, C., Hauglustaine, D., Li, B., Liu, J., Zhou, F., and Tao, S.: Influence of anthropogenic aerosol deposition on the relationship between oceanic productivity and warming, Geophysical Research Letters, 42, 10,745–10,754, doi:10.1002/2015GL066753, http://dx.doi.org/10.1002/2015GL066753, 2015GL066753, 2015.

Zhang, J., Campbell, J. R., Hyer, E. J., Reid, J. S., Westphal, D. L., and Johnson, R. S.: Evaluating the impact of multisensor data assimilation on a global aerosol particle transport model, Journal of Geophysical Research: Atmospheres, 119, 4674–4689, doi:10.1002/2013JD020975, http://dx.doi.org/10.1002/2013JD020975, 2013JD020975, 2014.